

Figure 1.4: The electromagnetic stirring.

frequently occur in the industrial operations such as

- the formation of oscillation marks on the steel surface;
- the generation of cracks on the longitude and transverse of surface and subsurface of steel;
- the breakout of molten steel from the bottom of the mould.

Thus, it is necessary to understand the phenomena occurring in the casting process in order to develop better casting technologies and optimize the process. Although a great deal of work has been carried out to study various aspects of the continuous casting process, very few attempts have been made to study the fluid flow and heat transfer in the meniscus region. The phenomena in this region are still not well understood. Thus, in this work, the meniscus region is included in the computational domain. The aims of this work are to establish a mathematical model for the fluid flow, heat transfer and solidification problem

Jutatip Archapitak Introduction / 6

and to develop a numerical algorithm for simulating the phenomena occurring in the meniscus region in the electromagnetic continuous casting process. In addition, the two-phase flow of steel and flux is studied to predict the meniscus shape. The effect of electromagnetic field on fluid flow and solidification of steel is investigated.

1.2 Scope and Objectives

Although various mathematical models have been developed to describe the phenomena occurring in the continuous casting process [3, 10, 11, 12, 13], the coupled fluid flow-heat transfer process in the meniscus region and the effect of electromagnetic field on the process have still not been fully understood. Thus, this research aims to

- develop a mathematical model to describe the coupled fluid flow and heat transfer with solidification process in the mould region and the meniscus region, taking into account the effect of the electromagnetic field;
- formulate the finite element methods for solving the electromagnetic stirring problem and the coupled fluid flow and heat transfer problem;
- develop a numerical algorithm for simulating the electromagnetic casting process;
- investigate the effect of electromagnetic field on the flow field, temperature field and meniscus shape.

1.3 Outline of the Thesis

This thesis comprises six chapters. In chapter 1, the basic principles of the continuous steel casting and the electromagnetic stirring technology are presented. The scope and objectives are also given in this chapter. In chapter 2, the previous works closely related to our scope and objectives are summarized. Chapter 3 concerns the mathematical model for studying the

two-dimensional electromagnetic stirring problem. The governing equations are Maxwell's equations. A numerical algorithm based on the finite element method is developed to solve the problem. The commercial package FEMLAB is also used to simulate the electromagnetic field in the continuous casting process. The effect of casting parameters such as source current and frequency of magnetic field on the electromagnetic force are investigated. In chapter 4, the effect of electromagnetic field on the coupled fluid flow and heat transfer process is studied. The governing equations consist of the Navier-Stokes equations, the continuity equation and the convection-diffusion equation. A numerical algorithm based on the finite element method is developed to solve the problem. The effect of various casting parameters and electromagnetic parameters on the flow field and temperature field are investigated. In chapter 5, we present a 2-D mathematical model of steel-flux flow in the meniscus region to predict the meniscus shape. An algorithm based on the pressure balance and the moving finite element method are developed to solve this problem. The effect of electromagnetic fields on the flow field is studied in this chapter.

The conclusions gained from this work are given in chapter 6, together with some suggestions for further work.

CHAPTER 2

LITERATURE REVIEW

2.1 General Overview

Many complex phenomena, such as solidification of steel, formation of oscillation marks on steel surface, breakout of molten steel at the bottom of the mould and flow of flux, occur in the continuous steel casting process. All these phenomena have effect on the quality of steel product. To improve the product quality, new technologies using electromagnetic field in the process have been developed to cast steel products.

Over the last few decades, extensive research has been carried out to study the various phenomena occurring in the continuous steel casting process, including experimental studies, analytical studies and numerical studies. Numerical investigation has been the dominant approach, as experimental studies are limited due to the high temperature involved in the process and analytical approach could only solve very simple problems. The previous studies mainly focused on the following areas [3, 6, 9, 15]:

- the meniscus phenomena,
- flux flow and formation of oscillation marks on the steel surface,
- heat transfer with solidification of steel,
- flow of molten steel,
- the coupled fluid flow and heat transfer,
- the effect of an electromagnetic field on molten steel flow and heat transfer with solidification.

2.2 Modelling of Fluid Flow and Heat Transfer

Various mathematical models and numerical algorithms for fluid flow and heat transfer have been developed to study the pattern of molten steel flow and the temperature distribution in the continuous steel casting process. In 1997, Li [14] developed a numerical algorithm based on the finite element method and the Lagrangian Eulerian formulation for solving the transient evolution of the fluid flow, heat transfer and solidification phenomena in the ingot and spreading casting. His model is based on Scheil's equation to predict temperature distribution and fluid flow of steel. His results lead to better understanding of the process and provide useful information which can be used to improve the design of the casting process and equipment. Wiwatanapataphee (1998) [3] presented a coupled turbulent fluid flow-heat transfer with solidification model to analyze the effect of turbulence on the solidification of steel and the flow of molten steel. She developed a finite element algorithm to solve the problem and investigated the effect of some casting parameters on the solidification profile and the flow field of fluid. Yang et al. (1998) [15] developed a coupled model for the fluid flow, heat transfer, solidification and solute redistribution in the continuous casting process. The porous media theory is used to model the blockage of fluid flow by columna dendrites in the mushy zone. The output shows the close relationship between the flow pattern of molten steel and the shape of the solid shell. In the work of Lee et al. (1999) [16], the finite difference method is used to analyze the turbulent fluid flow in a round billet and the finite element method is used to analyze the thermo-elastic plastic deformation. The simulation results are in good agreement with the experimental observations. The cracks on surface were predicted in the work and the effect of casting speed was investigated. In 2001, Takatani et al. [17] developed a mathematical model for simulating the transient fluid flow in a continuous casting mould. The argon gas injected from the nozzle, the molten steel and the solidified shell are all taken into account in the calculation. They also used a water model in their experimental study and compared experimental results with the simulation results. An algorithm based

on the SOLA method was used to solve the problem. In 2002, Thomas *et al.* [18] presented four different methods for evaluating velocity of fluid flow in the liquid pool. The computations are based on PIV, CFX and LES, and electromagnetic sensors at the mould wall are used to measure the flow velocity. The turbulence effect is modelled by using the standard $K - \varepsilon$ model.

2.3 Modelling of Electromagnetic Field in Continuous Casting Process

Major reviews on the application of electromagnetic field in the continuous casting process are given in many papers due to Birat and Chonè (1983) [6], Garnier (1990) [19], Kolesnichenko (1990) [20] and Nakanishi (1996) [21]. Various studies have been undertaken to develop mathematical models and numerical algorithms to study the electromagnetic problem in the continuous casting process. Makarov et al. (2000) [22] analyzed the conventional method for electromagnetic separation of small inclusion in metal casting with high electric conductivity. The separation technique for the electromagnetic force was presented and analyzed in each case. It is noted that a direct current superconduction coil can drastically improve the power loss in the process. Trindade et al. (2002) [23] introduced a low-frequency numerical model for the electromagnetic field in the continuous casting process. A finite element algorithm based on the ELEKTRA/OPERA-3D Package was used to solve the problem. They compared the simulation outputs with experimental measurements and the results were in agreement. In the same year, Na et al. (2002) [24] used a high frequency magnetic field in a soft contact continuous casting mould in the continuous steel casting process. The distribution of electromagnetic field, the electromagnetic body force and the effect of magnetic field frequency on the solidification were discussed in their work.

2.4 Modelling of Fluid Flow and Heat Transfer at the Presence of an Electromagnetic Field

Over the last two decades, the electromagnetic casting has been developed to cast steel products. In 1989, the influence of an electromagnetic field on the solidification was investigated in the work of Miyoshino et al. [9]. They introduced the fundamental of magnetohydrodynamic phenomena through experimental and numerical studies. A low frequency magnetic field (60 Hz) was used in the experimental system. In the same year, Ganma et al. [25] studied the pattern of fluid flow in the mould with the effect of electromagnetic stirring in the slab caster. The experimental results and the simulation results were given in the work. The results show that the velocity of molten steel that is injected from the nozzle is decelerated when the electromagnetic field is applied. In 1996, Trophime et al. [26] presented a mathematical model for the magnetrohydrodynamic problem. The electromagnetic model $(A - \phi \text{ model})$ and the fluid flow model are developed and the finite element method is used to solve the problem. In 1997, Toh et al.[8] presented a mathematical model for controlling the solidification of steel in the continuous steel casting process with the effect of electromagnetic field. The low-frequency magnetic field used in the simulation was of 60 Hz. The numerical results show that the surface of the steel is improved by the use of the magnetic field. As in the works of Fujisaki et al. [27, 28], they presented the mathematical model for In-Mold electromagnetic stirring in the continuous casting process. The experimental results and simulation results are in good agreement and show that the electromagnetic stirring leads to more uniform velocity field near the mould wall. In 1998, Li [29] used an electromagnetic field in a model for the coupled fluid flow, heat transfer and solidification process. Maxwell's equations were used to model the electromagnetic field. The results show that an electromagnetic field can reduce the fluid motion and affect the quality of the steel. Dumont and Gagnoud (2000) [30] presented a model for the molten metal shape in the electromagnetic casting to analyze the interactions between the shape of a molten metal and a magnetic field distribution. They developed a numerical algorithm based on a moving finite element mesh with impedance boundary condition to solve the problem, and determined the free surface under the equilibrium of the electromagnetic and hydrostatic pressures. Fujisaki (2000) [31] developed a three-dimension magnetohydrodynamic calculation model for the heat transfer and solidification problem. The electromagnetic force is calculated using the shadow method when the flow of molten steel changes. The results of this calculation show that the electromagnetic stirring makes the solidified steel shell uniform and the dynamic deviation of temperature stable. Li et al. (2000) [32] developed a mathematical model for the fluid flow with the effect of an electromagnetic field. The effect of argon gas injection was also investigated in this work. The computational results show that the argon gas injection affects the flow pattern of molten steel. In 2001, Park et al. [33] presented a mathematical model for the fluid flow and heat transfer analysis. The effect of varying the nozzle angle is taken into account to investigate the flow pattern in the mould. In 2002, Park et al. [34] and Kim et al. [35] studied the effect of a high frequency magnetic field in the electromagnetic casting technology. The experimental study was carried out to examine the effect of mould shape on the quality of the steel billet surface. They also investigated the effect of current source, casting speed and mould oscillation pattern on the surface quality of steel.

2.5 Modelling of Meniscus Phenomena

The study of the meniscus phenomena in the continuous casting process has been undertaken by many researchers. The flow of molten steel, lubrication flux, and heat transfer at the top surface were studied by McDavid and Thomas (1996) [36]. A three-dimensional finite element formulation was presented in their work. The effect of various material parameters on the formation of the flux layer was also investigated. The model gave reasonable results of the flux layer in the operating slab casting. The melting behavior of mould powders and the formation of the mould powder liquid pool were studied by Nakano et al. [37] in

1970. They proposed a one-dimensional heat conduction equation taking into account the difference in material properties of the various forms of the flux. In the work of Nakata and Etay (1992)[38], the two-dimensional meniscus shape under an alternating magnetic field was simulated. The finite difference method was used to solve the problem. The frequency of magnetic field and coil current are taken into account to investigate the height of meniscus layer. Li et al. (1995) [39] studied the behavior on the meniscus region and the properties of the surface on the billet casting in the presence of a magnetic field. The relations between the meniscus behavior and the surface quality were investigated in their work. The effect of a high-frequency magnetic field, mould oscillation on meniscus behavior was presented. The experimental results using molten gallium and molten tin were used to confirm the given concepts. The results of the study also showed that the use of a magnetic field improves the quality of the steel surface. Lucus (1998) [40] proposed a three-dimensional model for the fluid flow problem. The meniscus interface was studied by using the commercial package CFX. His results gave a flow field similar to that simulated using PIV by Thomas (2001) [41]. Sha et al. (1996) [42] investigated the behavior of meniscus on the mercury and silicon oil with the effect of oscillation wall. A two-dimensional mathematical model was presented in the work, together with the initial and boundary conditions. The Marker and Cell (MAC) method has been used to solve the problem. The experimental results and the computation results on the meniscus shape were in good agreement.

2.6 Concluding Remarks

Many models concerning about the phenomena in the continuous casting process have been developed to describe the complex phenomena. Many researchers focused only on subproblems of heat transfer, fluid flow and solidification. Further work is needed to investigate the influence of electromagnetic field on the coupled fluid flow and heat transfer with solidification process occurring in the continuous steel casting process.

CHAPTER 3

ELECTROMAGNETIC FIELD IN CONTINUOUS CASTING PROCESS

3.1 General Overview

Over the last few decades, the electromagnetic continuous casting process, as shown in Figure 1.4, has been used to cast steel products. The electromagnetic field will generate eddy currents and electromagnetic forces which consequently influence the flow of molten steel and heat transfer with solidification. As steel is a good conductor, the magnetic Reynold's number is very small. The change in the magnetic flux density caused by the fluid flow can thus be neglected. Hence, the electromagnetic problem is uncoupled from the fluid flow problem and solved separately.

In this chapter, we establish a mathematical model for the electromagnetic problem in the continuous casting process. The $A - \phi$ model based on Maxwell's equations and boundary conditions are presented in section 3.2. In section 3.3, the Bubnov-Galerkin finite element method for the solution of the electromagnetic problem is presented. In section 3.4, the influences of various parameters on the electromagnetic field in the continuous casting process are investigated.

3.2 Boundary Value Problem for the Electromagnetic Field

The governing equations for the electromagnetic field include the Maxwell's equations and the constitutive equations. Let H and E denote respectively the magnetic field and the electric field. The Maxwell's equations are

$$\nabla \times \mathbf{H} = \mathbf{J} + \frac{\partial \mathbf{D}}{\partial t},\tag{3.1}$$

Fac. of Grad. Studies, Mahidol Univ.

$$\nabla \times \mathbf{E} = -\frac{\partial \mathbf{B}}{\partial t},\tag{3.2}$$

$$\nabla \cdot \mathbf{B} = 0, \tag{3.3}$$

$$\nabla \cdot \mathbf{D} = \rho_d, \tag{3.4}$$

where \mathbf{J} is the total current density, \mathbf{D} is the electric displacement, ρ_d is the free charge density, and \mathbf{B} is the magnetic flux density. The magnetic flux density \mathbf{B} and the electric displacement \mathbf{D} are respectively related to the magnetic field \mathbf{H} and the electric field \mathbf{E} by the following constitutive equations

$$\mathbf{B} = \mu \mathbf{H},\tag{3.5}$$

$$\mathbf{D} = \varepsilon \mathbf{E},\tag{3.6}$$

where μ and ε are magnetic permeability and electric permeability, respectively. Another constitutive equation relating the induced current density with **E**, **B** and the velocity **v** is as follows

$$\mathbf{J_e} = \sigma(\mathbf{E} + \mathbf{v} \times \mathbf{B}) + \rho_d \mathbf{v},\tag{3.7}$$

where σ is the electric conductivity. For metal material (good conductors), we could assume that the field changed in one part of the system radiates to other parts instantaneously. Thus, the term $\frac{\partial \mathbf{D}}{\partial t}$ in the equation (3.1) can be neglected and the equation (3.1) becomes

$$\nabla \times \mathbf{H} = \mathbf{J},\tag{3.8}$$

from which and noting that the divergence of the curl of a vector field is identical to zero, we have

$$\nabla \cdot \mathbf{J} = 0. \tag{3.9}$$

Furthermore, in the case that the magnetic Reynolds number $(R_m = \mu \sigma \mathbf{v} L)$ is sufficiently small ($\ll 1$), the term $(\mathbf{v} \times \mathbf{B})$ in equation (3.7) due to fluid flow can be neglected. Under the above approximation and neglecting the displacement current ρ_d , the field equations are simplified as follows

$$\nabla \times \mathbf{H} = \mathbf{J},\tag{3.10}$$

$$\nabla \times \mathbf{E} = -\frac{\partial \mathbf{B}}{\partial t},\tag{3.11}$$

$$\nabla \cdot \mathbf{B} = 0, \tag{3.12}$$

$$\nabla \cdot \mathbf{D} = 0, \tag{3.13}$$

$$\mathbf{B} = \mu \mathbf{H},\tag{3.14}$$

$$\mathbf{J_e} = \sigma \mathbf{E}.\tag{3.15}$$

The Maxwell's equations and the constitutive equations can also be formulated in terms of potential functions. From equation (3.12) and noting that the divergence of the curl of a vector field is identical to zero, we can introduce the magnetic flux density \mathbf{B} in terms of a magnetic vector potential \mathbf{A} such that

$$\mathbf{B} = \nabla \times \mathbf{A}.\tag{3.16}$$

Using equations (3.14) and (3.16), we have from equation (3.10) that

$$\nabla \times (\frac{1}{\mu} \nabla \times \mathbf{A}) = \mathbf{J}. \tag{3.17}$$

Substituting equation (3.16) into equation (3.11), we have

$$\nabla \times (\mathbf{E} + \frac{\partial \mathbf{A}}{\partial t}) = 0. \tag{3.18}$$

Thus, the field $\mathbf{E} + \frac{\partial \mathbf{A}}{\partial t}$ is conservative and consequently there exists a scalar potential ϕ such that

$$\mathbf{E} + \frac{\partial \mathbf{A}}{\partial t} = -\nabla \phi. \tag{3.19}$$

Hence, the electric field can be determined by

$$\mathbf{E} = -\frac{\partial \mathbf{A}}{\partial t} - \nabla \phi. \tag{3.20}$$

The total current density J is defined as the sum of the induced current density J_e and the source current density J_s , namely

$$\mathbf{J} = \mathbf{J_e} + \mathbf{J_s} = -\sigma \frac{\partial \mathbf{A}}{\partial t} - \sigma \nabla \phi + \mathbf{J_s}.$$
 (3.21)

Substituting equation (3.21) into (3.17), we end up with the Maxwell's equations in terms of the magnetic vector potential \mathbf{A} and the electric scalar potential ϕ as follows

$$\nabla \times (\frac{1}{\mu} \nabla \times \mathbf{A}) = -\sigma \frac{\partial \mathbf{A}}{\partial t} - \sigma \nabla \phi + \mathbf{J_s}, \tag{3.22}$$

$$\nabla \cdot (-\sigma \frac{\partial \mathbf{A}}{\partial t} - \sigma \nabla \phi + \mathbf{J_s}) = 0. \tag{3.23}$$

In the case that sinusoidal current is applied for the problem, the solution may be assumed to have the form of $\mathbf{A}(\mathbf{x})e^{j\omega t}$. Thus, the partial derivative of the vector potential with respect to time may be replaced by $j\omega \mathbf{A}$. Hence equations (3.22) and (3.23) become

$$\nabla \times (\frac{1}{\mu} \nabla \times \mathbf{A}) = -\sigma j \omega \mathbf{A} - \sigma \nabla \phi + \mathbf{J_s}, \tag{3.24}$$

$$\nabla \cdot (-\sigma j\omega \mathbf{A} - \sigma \nabla \phi + \mathbf{J_s}) = 0. \tag{3.25}$$

These equations with a set of suitable boundary conditions describe the general 3-D electromagnetic field. Based on the FEMLAB user guide [43], the gauge transformation is applied to obtain the unique solution of the system. Let \mathbf{A} and ϕ be the solutions, the fields $\widetilde{\mathbf{A}} = \mathbf{A} + \nabla \mathbf{\Psi}$ and $\widetilde{\phi} = \phi - j\omega \mathbf{\Psi}$ also satisfy the equations for any scalar field $\mathbf{\Psi}$ such chosen that $\widetilde{\mathbf{A}}$ and $\widetilde{\phi}$ satisfy the boundary conditions. The system of equations can be reduced by choosing $\mathbf{\Psi} = -\frac{j\phi}{\omega}$, as for this case, $\widetilde{\mathbf{A}} = \mathbf{A} - \frac{j}{\omega} \nabla \phi$ and $\widetilde{\phi} = 0$. The particular choice of $\mathbf{\Psi}$ fixes the gauge and makes $\widetilde{\mathbf{A}}$ unique. The electric field and magnetic field are not affected by this choice of gauge, hence we can reduce the system to one equation as follows

$$\nabla \times (\frac{1}{\mu} \nabla \times \mathbf{A}) = -\sigma j \omega \mathbf{A} + \mathbf{J_s}. \tag{3.26}$$

In the real world applications, many problems, such as axisymmetric problems and the problem of one dimension being very large in comparision with others, can be modelled as two dimensional. For rectangular (x, y, z) coordinates, we can construct an approximate two-dimensional model to describe the electromagnetic field on the plane parallel to the x-z plane. For this case, Let $\mathbf{A} = (0, A_y(x, z), 0)$ and $\mathbf{J} = (0, J_y(x, z), 0)$, and $\phi = constant$. Thus,

$$\nabla \times \mathbf{A} = \left(-\frac{\partial A_y}{\partial z}, 0, \frac{\partial A_y}{\partial x}\right),\tag{3.27}$$

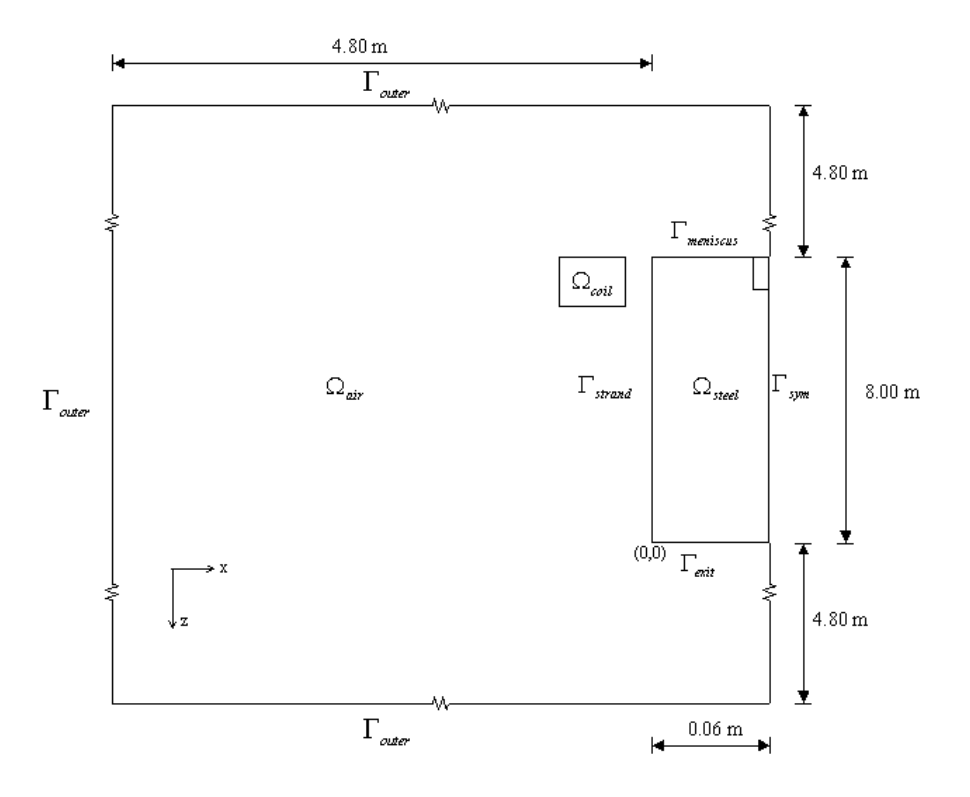


Figure 3.1: The computation domain for the electromagnetic problem.

$$\nabla \times (\nabla \times \mathbf{A}) = (0, -\nabla^2 A_y, 0). \tag{3.28}$$

Hence, equation (3.22) becomes

$$\sigma \mu \frac{\partial A_y}{\partial t} = \nabla^2 A_y - \mu J_{s_y}. \tag{3.29}$$

For the case of sinusoidal current, we let $A_y=A_ye^{i\omega t}$ and consequently equation (3.24) becomes

$$\sigma\mu\omega j A_y = \nabla^2 A_y - \mu J_{s_y}. \tag{3.30}$$

For the continuous casting problem, we consider a typical computation domain as shown in Figure 3.1. On the symmetric plane, the restriction that the magnetic flux cannot penetrate the face is imposed. This means $A_y = 0$ on the symmetric boundary. On the outer boundary, the vector potential are all set to zero. This implies that the effect of an inductor on the magnetic field at these points is negligible. An appropriate distance from the inductors is needed to insure high accuracy.

Fac. of Grad. Studies, Mahidol Univ.

In summary, the boundary value problem of the two-dimensional electromagnetic field is as follows

BVP: Find A_y such that the field equation (3.30) is satisfied in the computation domain Ω and all boundary conditions are satisfied.

3.3 Finite Element Method for the Electromagnetic Field

Firstly, we consider the general case, namely, the problem governed by equation (3.29). To solve this problem by the finite element method, we need to develop a variational statement of the problem. For this purpose, we multiply both sides of equation (3.29) by the test function and then integrate over Ω , namely

$$\left(\sigma\mu\frac{\partial A_y}{\partial t}, W_A\right) = ((A_{y,j})_{,j}, W_A) - (\mu J_{s_y}, W_A), \tag{3.31}$$

where (\cdot,\cdot) denotes the inner product on space $L^2(\Omega)$. As

$$W_A \nabla^2 A_y = \nabla \cdot (W_A \nabla A_y) - \nabla W_A \cdot \nabla A_y, \tag{3.32}$$

substituting equation (3.32) into equation (3.31) yields

$$\int_{\Omega} \sigma \mu \frac{\partial A_y}{\partial t} W_A d\Omega = -\int_{\Omega} (\nabla W_A) \cdot (\nabla A_y) d\Omega + \int_{\Gamma} W_A \nabla A_y \cdot \mathbf{n} \, d\mathbf{s} - \int_{\Omega} \mu J_{s_y} W_A d\Omega.$$
(3.33)

By choosing $W_A = 0$ on the boundary where $A_y = 0$, we have

$$\int_{\Omega} \sigma \mu \frac{\partial A_y}{\partial t} W_A d\Omega = -\int_{\Omega} (\nabla W_A) \cdot (\nabla A_y) d\Omega - \int_{\Omega} \mu J_{s_y} W_A d\Omega, \tag{3.34}$$

or

$$\left(\sigma\mu\frac{\partial A_y}{\partial t}, W_A\right) = (A_{y,j}, W_{A,j}) - (\mu J_{s_y}, W_A). \tag{3.35}$$

Thus, the variational statement for the problem is as follows

VBVP: Find $A_y \in H_0^1(\Omega)$ such that for all the test function $W_A \in H_0^1(\Omega)$, equation (3.35) holds, where $H_0^1(\Omega) = \{v \in H^1(\Omega) | v = 0 \text{ on } \partial\Omega\}$.

To solve this problem numerically, we pose the problem into an N-dimensional subspace A_y and W_A , namely approximate A_y and W_A by

$$A_y = \sum_{i=1}^{N} (A_y)_i \phi_i$$
 , $W_A = \sum_{k=1}^{N} (W_A)_k \phi_k$. (3.36)

Substituting equation (3.36) into equation (3.35), we have

$$\left\{ \left(\sigma \mu \frac{\partial A_y}{\partial t}, \phi_k \right) + \left(A_{y,j}, \phi_{k,j} \right) + \left(J_{s_y}, \phi_k \right) \right\} W_{A_k} = 0,$$
(3.37)

where k = 1, 2, ..., N and j = 1, 2. Then,

$$\sum_{i=1}^{N} (\sigma \mu \phi_i, \phi_k) \frac{\partial A_{y_i}}{\partial t} + \sum_{i=1}^{N} (\phi_{i,j}, \phi_{k,j}) A_{y_i} = -(J_{s_y}, \phi_k), \tag{3.38}$$

which can be written in matrix form as

$$\mathbf{M}\frac{\partial \mathbf{A_y}}{\partial t} + \mathbf{L}\mathbf{A_y} = \mathbf{F},\tag{3.39}$$

where

$$\mathbf{M} = \{m_{ik}\}\ \text{with}\ m_{ik} = (\sigma \mu \phi_i, \phi_k) = \int_{\Omega} \sigma \mu \phi_k \phi_i d\Omega,$$

$$\mathbf{L} = \{L_{ik}\}$$
 with $l_{ik} = (\phi_{i,j}, \phi_{k,j}) = \int_{\Omega} \phi_{i,j} \phi_{k,j} d\Omega$,

$$\mathbf{F} = \{f_k\} = -(J_{s_y}, \phi_k) = -\int_{\Omega} \phi_k J_{s_y} \ d\Omega.$$

For the time-harmonic problem, the first term of equation (3.38) can be written as

$$\sum_{i=1}^{N} (j\omega\sigma\mu\phi_i, \phi_k) A_{y_i}.$$
(3.40)

Therefore, we have

$$\sum_{i=1}^{N} \left[\left(j\omega \sigma \mu \phi_i, \phi_k \right) + \left(\phi_{i,j}, \phi_{k,j} \right) \right] A_{y_i} = -(J_{s_y}, \phi_k), \tag{3.41}$$

which can be written in the matrix form as

$$\overline{\mathbf{M}}\mathbf{A}_{\mathbf{y}} = \mathbf{F},\tag{3.42}$$

where

$$\overline{\mathbf{M}} = \{m_{ik}\}$$
 with $m_{ik} = \int_{\Omega} (j\omega\sigma\mu\phi_i\phi_k + \phi_{i,j}\phi_{k,j}) d\Omega$.

Once A_y is determined by solving the linear system of equation (3.42), **B** and $\mathbf{J_e}$ can be determined from equations (3.16) and (3.21) and consequently the electromagnetic force at each node can be determined by $\mathbf{F_{em}} = \mathbf{J_e} \times \mathbf{B}$.

3.4 Numerical Studies

The example under the investigation is a square billet continuous caster which has a width of 0.12 m and a depth of 0.8 m. The computation domain for this problem is given in Figure 3.1. The finite element mesh, constructed from FEMLAB, has 23180 elements and 11856 nodes as shown in Figure 3.2. The parameters used in this problem is as given in Table 3.1. The computation schemes for investigating the effect of varying current source and frequency of magnetic field on the electromagnetic force are given in Table 3.2. The computation results are shown in Figure 3.3-3.7.

Figure 3.3 shows the contour plot of the magnetic vector potential A_y (Wb/m) in the computation domain. All values of magnetic vector potential are negative. Negative values mean sign of values gives the same direction as the source current. It indicates that the magnitude of A_y is between 0 and 0.004 Wb/m which reduces 60% from the original source (coil) to the steel strand while it reduces only 20% to environment.

Figure 3.4 shows the vector plot of the magnetic flux density corresponding to the magnetic vector potential obtained from Figure 3.3. The distribution of the magnetic flow field corresponds to the right hand spiral rule (RHS). The magnitude of the magnetic flux in the steel strand is larger than that in the environment because of the higher electric conductivity.

The contour plot of induce currents in the molten steel pool is shown in Figure 3.5. Its direction is in the opposite way of the source current. The magnitude of \mathbf{J}_e is between 0 and $1.14 \times 10^5 A/m^2$. Its value reduces almost 100% from strand surface to the symmetry plane because we assume that the magnetic flux cannot penetrate to the symmetry plane.

Figure 3.6 shows the vectors plot of the electromagnetic force generated

by the magnetic field and the induced current in the steel. The direction of the electromagnetic force is in-mould direction. The electromagnetic flux flows into the mould with higher intensity in the top part of mould than that in other parts. There is no significant electromagnetic force present at 3 meters below the meniscus. It is noted that the magnitude of the electromagnetic force decreases with the increase of distance from the mould wall.

The effect of source current on the intensity of electromagnetic force is investigated by using three different source current densities those are 1000000 A/m^2 , 2000000 A/m^2 and 3000000 A/m^2 . The results as shown in Figure 3.7 indicate that the larger source current generates the larger magnitude of electromagnetic force. By increasing the source current from 1000000 A/m^2 to 3000000 A/m^2 in a horizontal section 0.05 meters below the meniscus, the magnitude of electromagnetic force increases about 89% on the strand surface. It is clear that the intensity of electromagnetic force decreases with decreasing the source current.

Figure 3.8 shows the effect of the frequency of magnetic field on the magnitude of electromagnetic force. The results of the investigation, by using three different frequencies of 60 Hz, 80 Hz and 100 Hz, indicate that the higher magnetic frequency generates the larger magnitude of electromagnetic force. By increasing the frequency of the magnetic field from 60 Hz to 100 Hz at 5 cm below meniscus, the magnitude of electromagnetic force increases about 56% on strand surface. It is noted that the magnitude of electromagnetic body force decreases with the decrease of the frequency of the magnetic field.

3.5 Concluding Remarks

The mathematical model for simulating the electromagnetic problem in the continuous casting process is governed by the $A - \phi$ model, derived from

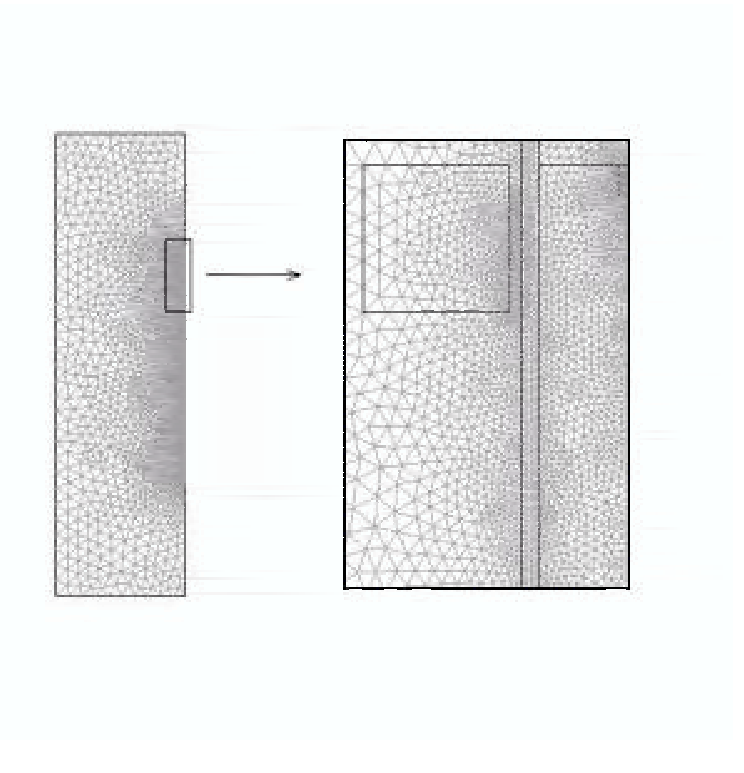


Figure 3.2: The finite element mesh for the electromagnetic problem.

Table 3.1: Material parameters

Parameter	Value	Unit
Conductivity of molten steel σ_s	7.14×10^5	$\Omega^{-1}m^{-1}$
Magnetic permeability in a vacuum μ	$4\pi \times 10^{-7}$	Henry/m
Magnetic permittivity in a vacuum ε	8.8541×10^{-12}	Farad/m

the Maxwell's equations. A finite element technique based on the Bubnov-finite element method is used to study the electromagnetic field in the continuous casting process.

The study shows that the electromagnetic force in molten steel generated by an external magnetic field directs toward the central plane

100

Scheme Source Current density Frequency J_s f $(Ampere/m^2)$ (Hz)1 1000000 60 2 200000060 3 3000000 60 4 2000000 80

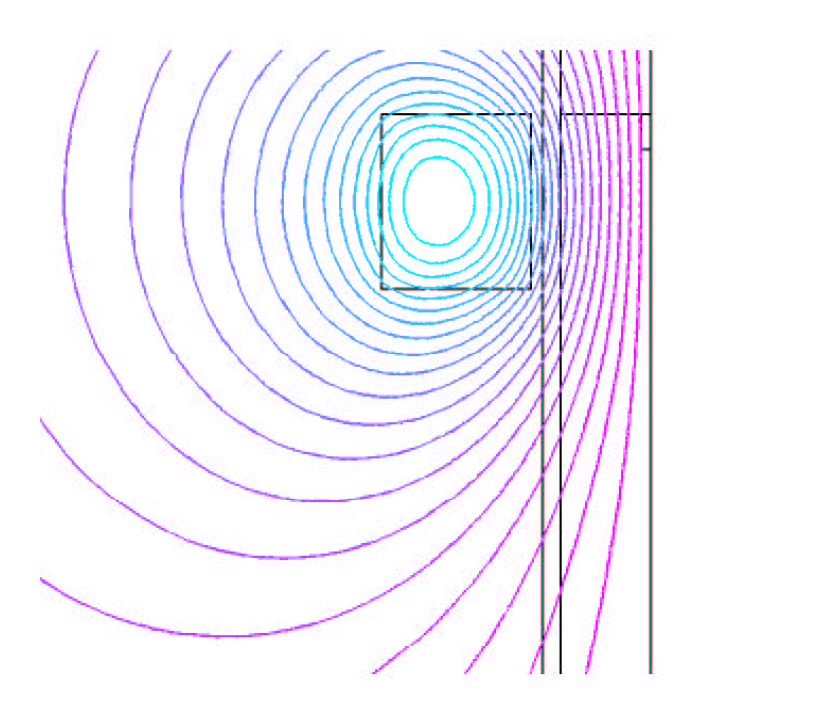
Table 3.2: Computation schemes

of the mould and its magnitude decreases with increasing distance from the mould wall. This force will contribute to the improvement of steel surface quality.

2000000

5

The study also shows that the source current density and the magnetic frequency have considerable effect on the magnitude of the electromagnetic force. By decreasing the source current density or the magnetic frequency, the magnitude of the electromagnetic force in the molten steel decreases significantly.



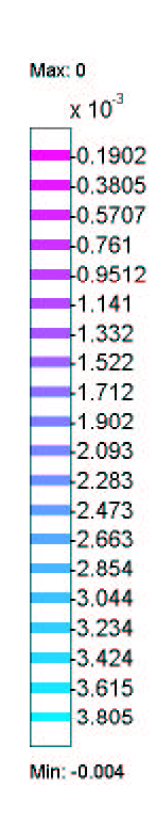


Figure 3.3: The contour plot of the magnetic vector potential $\mathbf{A}(Wb/m)$ at frequency f=60 Hz and source current density $\mathbf{J_s}=1000000~A/m^2$.

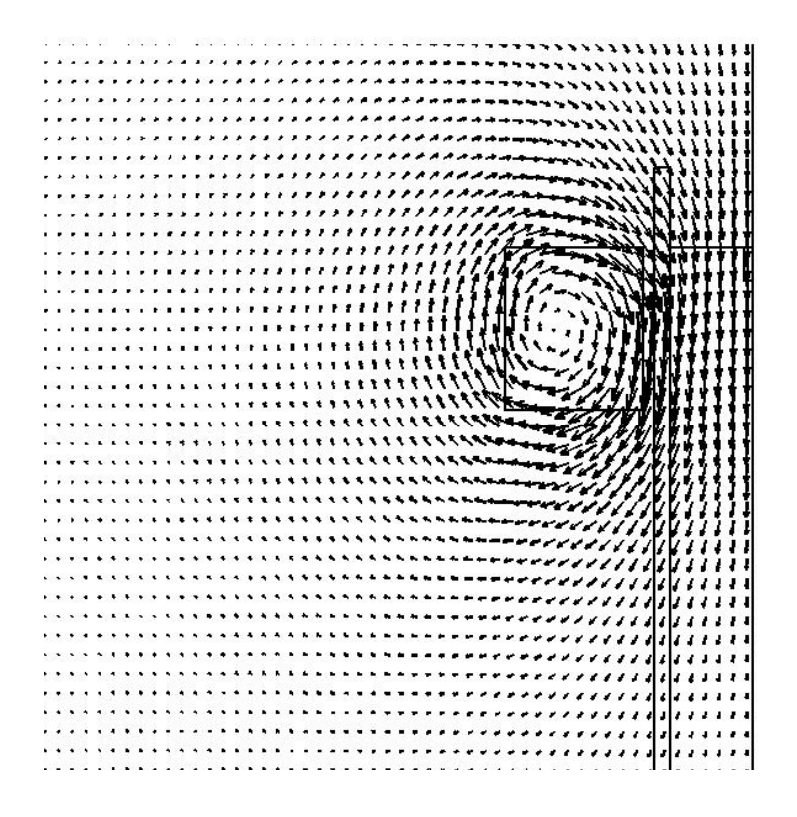


Figure 3.4: The vector plot of the magnetic flux density ${\bf B}$ (Tesla) at frequency f=60 Hz and source current density ${\bf J_s}=1000000~A/m^2$.

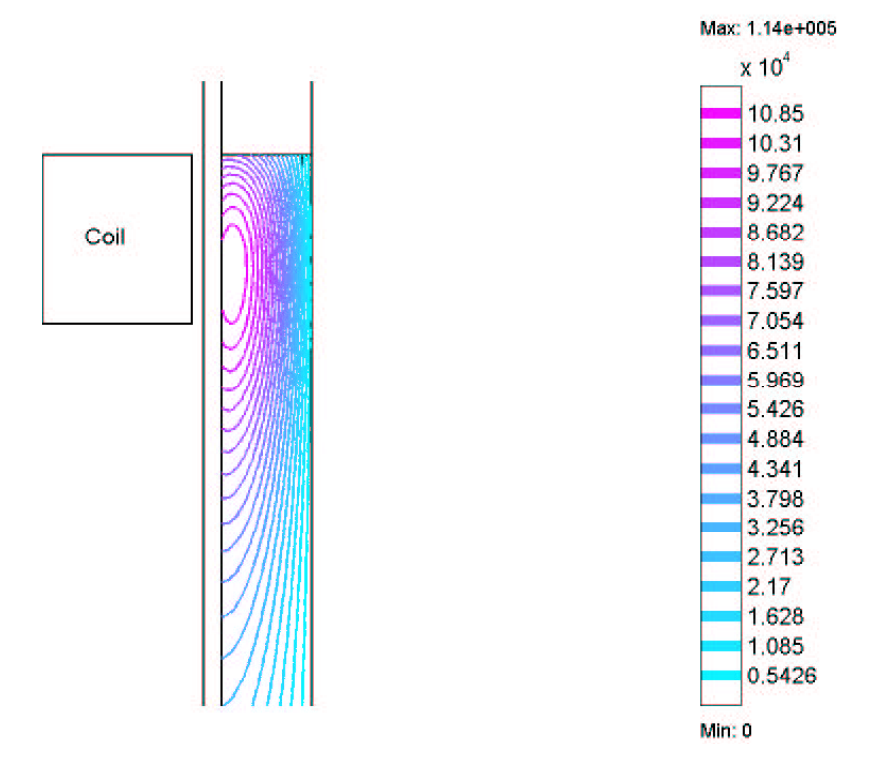


Figure 3.5: The contour plot of induced current ${\bf J_e}\,(A/m^2)$ in the continuous casting mould at frequency f=60 Hz and source current density ${\bf J_s}=1000000~A/m^2.$

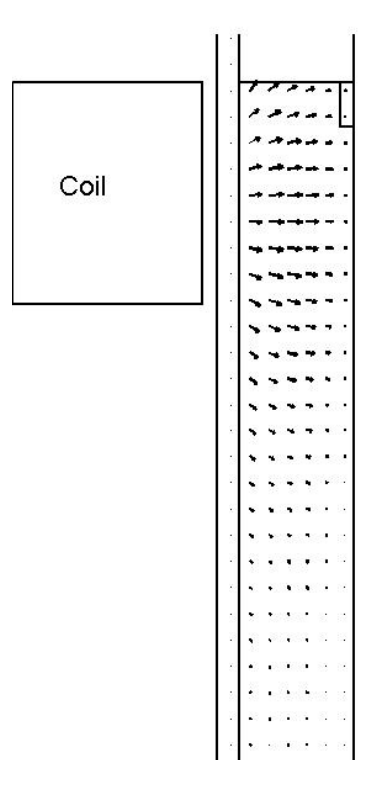


Figure 3.6: The vector plot of electromagnetic force F_{em} (N/m^3) in the electromagnetic continuous caster at frequency f=60 Hz and source current density $\mathbf{J_s}=1000000~A/m^2$.

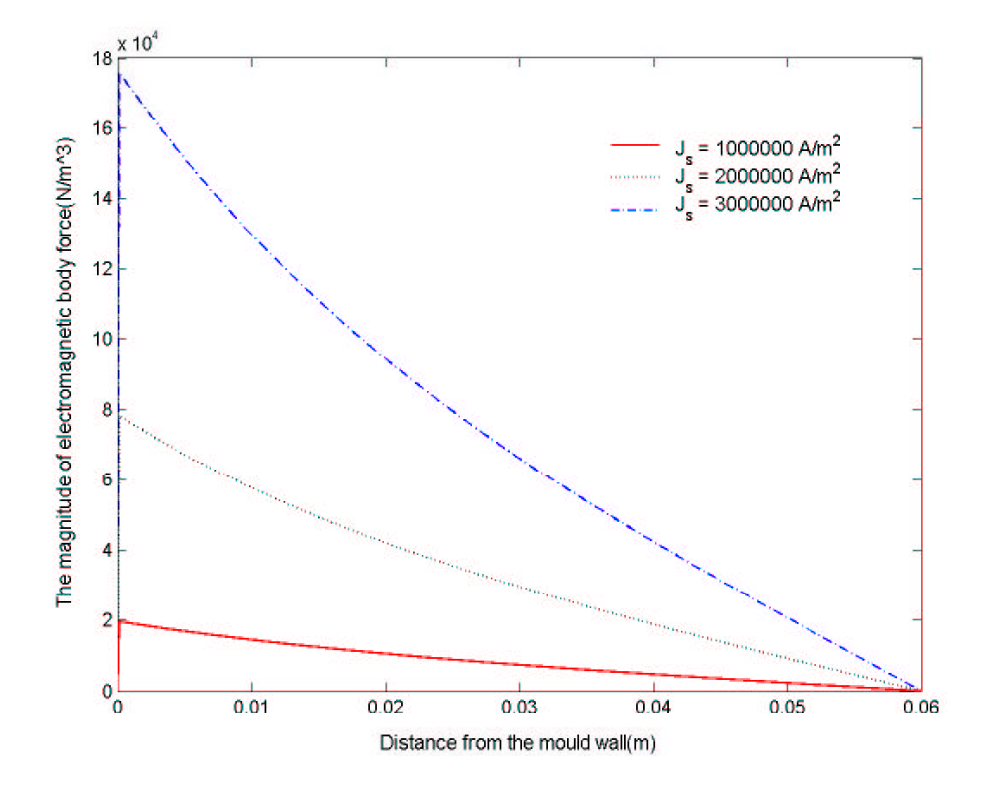


Figure 3.7: The influence of source current density $J_s\left(A/m^2\right)$ on the magnitude of electromagnetic force in the continuous casting process at frequency $f=60~\mathrm{Hz}$.

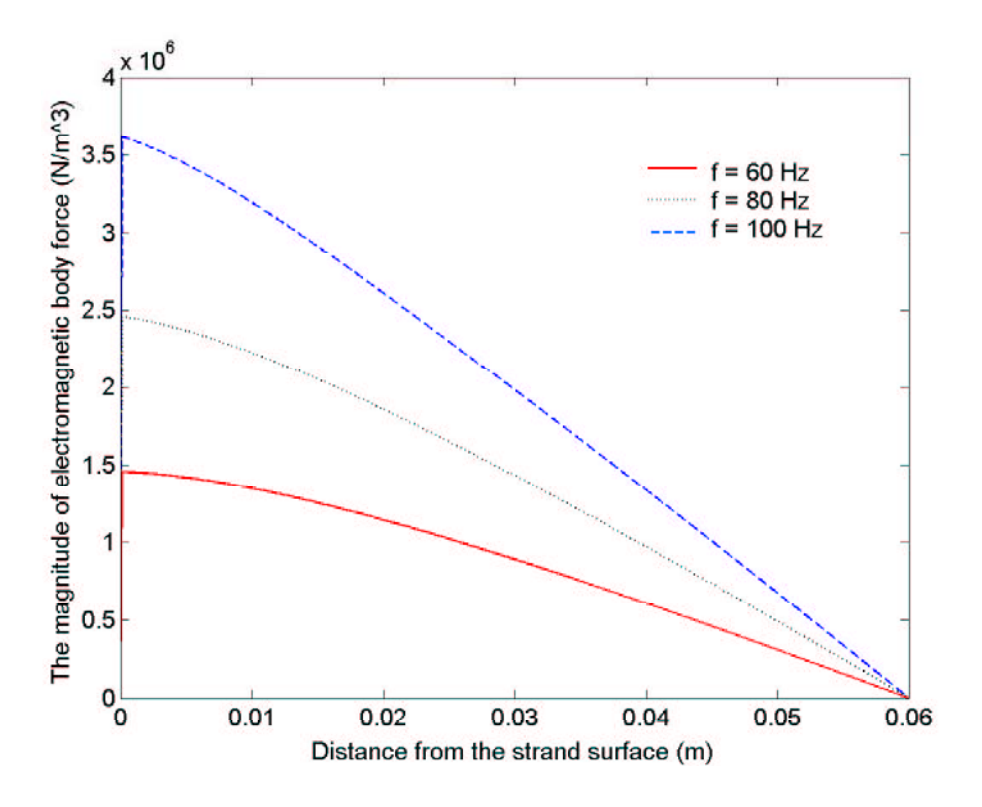


Figure 3.8: The influence of the frequency of magnetic field f(Hz) on the magnitude of electromagnetic force in the continuous casting process at source current density $\mathbf{J_s} = 1000000~A/m^2$.

CHAPTER 4

COUPLED FLUID FLOW-HEAT TRANSFER IN ELECTROMAGNETIC CASTING

4.1 General Overview

The electromagnetic continuous casting process has been developed to cast steel over the last few decades. Various mathematical models and numerical algorithms have been developed to simulate the heat transfer, fluid flow and electromagnetic stirring occurring in the casting process. A number of commercial packages, such as FIDAP, PHONIC, PIV, SOLA, OPERA-3D and MORDY, have been used for the simulation. However, only a few attempts have been made to study the coupled fluid flow, heat transfer and solidification problem taking into account the effect of electromagnetic stirring.

As the effect of molten steel flow on the magnetic flux density is negligible, the electromagnetic problem is decoupled from the fluid flow problem and is solved in chapter 3. The influence of electromagnetic field on the coupled fluid flow-heat transfer process is taken into account by adding the electromagnetic force to the fluid flow model. The molten steel is assumed to be an incompressible Newtonian fluid and the flow in the mushy region is modelled on the basis of Darcy's flow in porous media. The influence of turbulence on the fluid flow and heat transfer process is taken into account in this work. A single domain enthalpy method is used for the heat transfer-solidification problem in the continuous casting process. The complete set of equations for the coupled fluid flow, heat transfer and solidification process at the presence of an electromagnetic field is presented in section 4.2. In section 4.3-4.4, a numerical algorithm based on a Bubnov-Galerkin finite element method is established. In

section 4.5, a numerical investigation is carried out to study the influence of electromagnetic field on the fluid flow, heat transfer and solidification process.

4.2 Mathematical Model

In this section, the mathematical model for the coupled fluid flow, heat transfer and solidification process occurring in the electromagnetic continuous casting process is described. The governing equations for the problem include the Navier-Stokes equations, the continuity equation and the energy equation. The effect of electromagnetic field and turbulence on the flow field and the temperature field are taken into account.

To simulate the heat transfer process, a single-domain enthalpy method is used. From the principle of energy conservation, the heat transfer in the region undergoing a phase change is

$$\rho \left(\frac{\partial H_t}{\partial t} + u_j H_{t,j} \right) = \left(k_0 T_{,j} \right)_{,j} \tag{4.1}$$

where $(\cdot)_{,j}$ denotes differentiation with respect to x_j , u_j represents the velocity component of fluid in the x_j direction, ρ and k_0 are respectively the density of steel and the thermal conductivity of steel. The enthalpy H_t is defined as the sum of sensible heat h = cT and latent heat H as follows

$$H_t = cT + H, (4.2)$$

where c is the specific heat of liquid steel and the latent heat H is defined by

$$H = \begin{cases} 0 & \text{if } T \leq T_S \\ L\left(\frac{T - T_S}{T_L - T_S}\right) & \text{if } T_S < T < T_L \\ L & \text{if } T \geq T_L \end{cases}$$

$$(4.3)$$

in which L is the latent heat of steel, T_s and T_l are respectively the solidification temperature and the melting temperature of steel.

Substituting equation (4.2) to equation (4.1), we have

$$\rho c \left(\frac{\partial T}{\partial t} + u_j T_{,j} \right) = (k_0 T_{,j})_{,j} - \rho \left(\frac{\partial H}{\partial t} + u_j H_{,j} \right). \tag{4.4}$$

From equation (4.3), it is obviously that the last term in equation (4.4) is equal to zero everywhere except in the region where phase-change occurs. Consequently, the equation can be applied to all the regions including the solid region, the mushy region and the liquid region and there are no conditions to be satisfied at the phase-change boundary. Thus, the heat transfer-phase change problem can be solved by using a single domain approach.

For the flow of fluid in the electromagnetic caster, the molten steel is assumed to be a incompressible Newtonian fluid. The influence of turbulence on the transport of momentum and energy is modelled by the addition of the turbulent viscosity μ_t to the laminar viscosity μ_0 and the turbulent conductivity k_t to the molecular conductivity k_0 , yielding the effective viscosity μ_f and the effective thermal conductivity k_f given by

$$\mu_f = \mu_0 + \mu_t, \qquad k_f = k_0 + k_t, \tag{4.5}$$

where $k_t = \frac{c\mu_t}{\sigma_t}$, σ_t is the turbulent Prandtl number [11, 13, 16, 44, 45]. To simulate the influence of an electromagnetic field on the flow field in the electromagnetic continuous casting process, the electromagnetic force \mathbf{F}_{em} is incorporated into the fluid flow model. The flow field in the mushy region is modelled by Darcy's law for porous media. Thus, the unified field equations governing the multi-phases heat transfer and fluid flow with turbulence and electromagnetic effects, for all the regions with or without phase change are as follows

$$u_{i,i} = 0, (4.6)$$

$$\rho \left(\frac{\partial u_i}{\partial t} + u_j u_{i,j} \right) + p_{,i} - (\mu_f(u_{i,j} + u_{j,i}))_{,j} = F_i(u_i, T) + \rho g_i + F_{em_i}, \tag{4.7}$$

$$\rho c \left(\frac{\partial T}{\partial t} + u_j T_{,j} \right) = (k_f T_{,j})_{,j} - \rho \left(\frac{\partial H}{\partial t} + u_j H_{,j} \right), \tag{4.8}$$

where Darcy's law for porous media [3, 44, 46] has been used for modeling the flow in the mushy region and $F_i(u_i, T)$ is determined by

$$F_i(u_i, T) = C \frac{\mu_f \left[1 - f(T)\right]^2}{\rho f(T)^3} (u_i - (U_{cast})_i)$$
(4.9)

in which f(T) is the local liquid fraction which is approximated by the linear function

$$f(T) = \begin{cases} 0 & \text{if } T \le T_S \\ \frac{T - T_S}{T_L - T_S} & \text{if } T_S < T < T_L. \\ 1 & \text{if } T \ge T_L \end{cases}$$

$$(4.10)$$

The electromagnetic force F_{em_i} in the Navier-stokes equations (4.7) can be determined by

$$F_{em_i} = (\mathbf{J_e} \times \mathbf{B})_i \tag{4.11}$$

which is calculated from the results in chapter 3.

Equations (4.6)-(4.8) do not constitute a closed system as both μ_f and k_f are related to an unknown function μ_t . Various models, such as the mixing-length type model, the one-equation model [47, 48] and the two-equation $(K-\varepsilon)$ model [3, 49, 50, 51, 52, 53], have been proposed for calculating μ_t . Launder [45] and Ferziger [54], based on a critical review, suggested that the simple mixing-length type model is suitable for most boundary-layer type flows in the absence of recirculation; the one-equation model can be used to model simple recirculation flow; but for more complex flow fields, the two-equation model should be used. As the flow field in the continuous casting mould is complex with circulation, μ_t is calculated by using the two equation $K - \varepsilon$ model. As the phase change is taken into account in the heat transfer problem, the computation region has three sub-regions including the solidified steel region, the mushy region and the molten steel region. Consequently, the standard $K-\varepsilon$ model, which is suitable for the far-wall highly turbulent region, cannot be applied to the problem for the continuous casting process. Thus, some Fac. of Grad. Studies, Mahidol Univ.

modification to the standard $K - \varepsilon$ model is needed. According to the work by Wiwatanapataphee [3], the low-Reynold number $K - \varepsilon$ model is used in this project for the turbulent flow of molten steel in the continuous casting process, namely

$$\rho\left(\frac{\partial K}{\partial t} + u_j K_{,j}\right) - \left(\left(\mu_0 + \frac{\mu_t}{\sigma_K}\right) K_{,j}\right)_{,j} = -\frac{\mu_t}{\sigma_t} \beta g_j T_{,j} + \mu_t G - \rho \varepsilon, \tag{4.12}$$

$$\rho\left(\frac{\partial\varepsilon}{\partial t} + u_{j}\varepsilon_{,j}\right) - ((\mu_{0} + \frac{\mu_{t}}{\sigma_{\varepsilon}})\varepsilon_{,j})_{,j} = C_{1}(1 - C_{3})\frac{\varepsilon\mu_{t}}{K\sigma_{t}}\beta g_{j}T_{,j} + C_{1}\frac{\varepsilon}{K}\mu_{t}G - \rho C_{2}f_{\varepsilon}\frac{\varepsilon^{2}}{K}, \qquad (4.13)$$

where $G = 2\epsilon_{ij}\epsilon_{ij}$ with $\epsilon_{ij} = \frac{u_{i,j} + u_{j,i}}{2}$. The constants involved in equations (4.5)-(4.13) are empirical constants. Extensive examination of turbulent flows has resulted in a recommended set of values for these constants [3, 50], namely $\sigma_t = 0.9$, $\sigma_k = 1$, $\sigma_{\varepsilon} = 1.25$, $C_1 = 1.44$, $C_2 = 1.92$, and $C_3 = 0.8$.

Equations (4.12)-(4.13) are used to accommodate the region with relatively low local turbulent Reynolds number and to reduce the effect of turbulent across the various sub-layers. The turbulent viscosity μ_t is determined by [3, 45, 54]

$$\mu_t = \frac{0.09 f_\mu \rho K^2}{\varepsilon},\tag{4.14}$$

where the generalized damping mechanism of turbulent transport in both the liquid and mushy regions f_{μ} is determined [3] by

$$f_{\mu} = \sqrt{f(T)} exp(-3.4/(1 + R_t/50)^2),$$
 (4.15)

where f(T) is the liquid fraction as defined before in equation (4.10), R_t denotes the local turbulent Reynolds number defined by

$$R_t = \frac{\rho K^2}{\mu \varepsilon}. (4.16)$$

To ensure that all the terms in equations (4.12)-(4.13) will not tend to infinity as K approaches zero in the near-wall region, the last term of the right hand side of

equation (4.13) includes a damping function f_{ε} defined by

$$f_{\varepsilon} = 1 - A_{\varepsilon} e^{-R_t^2},\tag{4.17}$$

where A_{ε} is a constant and is chosen as one if $K < 10^{-4}$ or otherwise $A_{\varepsilon} = 0.3$ [3, 55, 56]. By choosing $A_{\varepsilon} = 1$ in equation (4.17), the term $\frac{\rho C_2 f_{\varepsilon} \varepsilon_2}{K}$ in equation (4.13) approaches zero as K becomes small. To completely define the problem, boundary and initial conditions for velocity, temperature, turbulent kinetic energy, and dissipation rate must be given. The computation region and the boundary conditions for the problem are shown in Figure 4.2, as detailed below. On the nozzle inlet Γ_{in} , the velocity, the temperature of steel, the turbulent kinetic energy and the rate of dissipation are respectively determined by

$$\mathbf{u} = \mathbf{u}_{in}, \quad T = T_{in}, \quad K = K_{in}, \quad \varepsilon = \varepsilon_{in}.$$
 (4.18)

On the solidified strand surface Γ_{wall} , the velocity is set to the casting speed, the heat transfer is determined by the convection boundary condition, the turbulent kinetic energy K and the rate of dissipation ε are assumed to be zero, namely

$$\mathbf{u} = (0, U_{cast}), \quad -k_f \frac{\partial T}{\partial \mathbf{n}} = h_{\infty} (T - T_{\infty}), \quad K = \varepsilon = 0.$$
 (4.19)

On the meniscus surface Γ_0 and the nozzle wall $\bar{\Gamma}_n$, the derivatives of the turbulent kinetic energy and the rate of dissipation in the normal direction are set to zero. The velocity is set to zero and the temperature is taken to be the inlet molten steel temperature, namely

$$\mathbf{u} = \mathbf{0}, \quad T = T_{in}, \quad \frac{\partial K}{\partial n} = \frac{\partial \varepsilon}{\partial n} = 0.$$
 (4.20)

On the plane of symmetry Γ_{sym} , the normal velocity \mathbf{v}_n is zero and the derivatives of the tangential velocity \mathbf{u}_t and temperature T in the normal direction are both zero; the derivatives of the turbulent kinetic energy and the rate of dissipation in the normal direction are also set to zero, namely

Fac. of Grad. Studies, Mahidol Univ.

$$\mathbf{u}_n = 0, \quad \frac{\partial \mathbf{u}_t}{\partial n} = \frac{\partial T}{\partial n} = 0, \quad \frac{\partial K}{\partial n} = \frac{\partial \varepsilon}{\partial n} = 0,$$
 (4.21)

where n is the unit vector normal to the boundary.

In summary, the boundary value problem for the turbulent fluid flow-heat transfer problem is as follows :

BVP: Find u_i, p, T, K and ε such that the field equations (4.6)-(4.8) and (4.12)-(4.13) are satisfied in the computation domain Ω and all boundary conditions (4.18)-(4.21) are satisfied.

4.3 Finite Element Formulation

To solve the BVP, firstly we use the penalty function method to weaken the continuity equation as follows

$$u_{i,i} = -\delta p^*, \tag{4.22}$$

where δ is a small positive number and p^* is denoted by

$$p^* = p - \rho gz. \tag{4.23}$$

The variational statement corresponding to the BVP can now be described as the following variational boundary value problem.

VBVP: Find u_i, p^*, T, K and $\varepsilon \in H^1(\Omega)$ such that for all w_i^u, w^p, w^T, w^K and $w^{\varepsilon} \in H_0^1(\Omega)$, all boundary conditions including (4.18)-(4.21) are satisfied and

$$(u_{i,i}, w^p) = (-\delta p^*, w^p),$$

$$(\frac{\partial u_i}{\partial t}, w^{u_i}) + (u_j u_{i,j}, w^{u_i}) - ((\frac{\mu_f}{\rho} (u_{i,j} + u_{j,i}))_{,j}, w^{u_i})$$

$$+ (\frac{1}{\rho} p_{,i}^*, w^{u_i}) = (\frac{1}{\rho} F_i, w^{u_i}) + (\frac{1}{\rho} F_{em_i}, w^{u_i}),$$

$$\left(\frac{\partial T}{\partial t}, w^{T}\right) + (u_{j}T_{,j}, w^{T}) - \left(\left(\frac{k_{f}}{\rho c}T_{,j}\right)_{,j}, w^{T}\right) = -\frac{1}{c}\left\{\left(\frac{\partial H}{\partial t}, w^{T}\right) + (u_{j}H_{,j}, w^{T})\right\},$$

$$\left(\frac{\partial K}{\partial t}, w^{K}\right) + (u_{j}K_{,j}, w^{K}) - \left(\left(\left(\frac{\mu_{0}}{\rho} + \frac{\mu_{t}}{\rho\sigma_{K}}\right)K_{,j}\right)_{,j}, w^{K}\right) = -\left(\frac{\mu_{t}}{\rho\sigma_{t}}\beta g_{j}T_{,j} - \frac{\mu_{t}}{\rho}G + \varepsilon, w^{K}\right),$$

$$\left(\frac{\partial \varepsilon}{\partial t}, w^{\varepsilon}\right) + (u_{j}\varepsilon_{,j}, w^{\varepsilon}) - \left(\left(\left(\frac{\mu_{0}}{\rho} + \frac{\mu_{t}}{\rho\sigma_{\varepsilon}}\right)\varepsilon_{,j}\right)_{,j}, w^{\varepsilon}\right) = \left(C_{1}(1 - C_{3})\frac{\varepsilon\mu_{t}}{K\rho\sigma_{t}}\beta g_{j}T_{,j}\right)$$

$$+ C_{1}\frac{\varepsilon\mu_{t}}{K\rho}G - C_{2}f_{\varepsilon}\frac{\varepsilon^{2}}{K}, w^{\varepsilon}, w^{\varepsilon}, w^{\varepsilon}$$

$$(4.24)$$

where $H^1(\Omega)$ is the Sobolev space $W^{1,2}(\Omega)$ with norm $||\cdot||_{1,2,\Omega}$, $H^1_0(\Omega) = \{v \in H^1(\Omega)|v=0 \text{ on } \partial\Omega_v \text{ where } \partial\Omega_v \text{ denote a Dirichlet type boundary for } v\}$, and the inner product (\cdot,\cdot) is defined by

$$(\mathbf{a}, \mathbf{b}) = \int_{\Omega} \mathbf{a} \cdot \mathbf{b} \ d\Omega. \tag{4.25}$$

Using Green's formula, the second order derivatives in (4.24) can be reduced to order one, namely

$$\left(\frac{1}{\rho}p_{,i}^{*}, w^{u_{i}}\right) = -\left(\frac{1}{\rho}p^{*}, w_{,i}^{u_{i}}\right) + B_{p}\left(w^{u_{i}}\right),$$

$$\left(\left(\frac{\mu_{f}}{\rho}\left(u_{i,j} + u_{j,i}\right)\right)_{,j}, w^{u_{i}}\right) = -\left(\left(\frac{\mu_{f}}{\rho}\left(u_{i,j} + u_{j,i}\right)\right), w_{,j}^{u_{i}}\right) + B_{u}\left(w^{u_{i}}\right),$$

$$\left(\left(\frac{k_{f}}{\rho c}T_{,j}\right)_{,j}, w^{T}\right) = -\left(\left(\frac{k_{f}}{\rho c}T_{,j}\right), w_{,j}^{T}\right) + B_{T}\left(w^{T}\right),$$

$$\left(\left(\left(\frac{\mu_{0}}{\rho} + \frac{\mu_{t}}{\rho \sigma_{K}}\right)K_{,j}\right)_{,j}, w^{K}\right) = -\left(\left(\left(\frac{\mu_{0}}{\rho} + \frac{\mu_{t}}{\rho \sigma_{K}}\right)K_{,j}\right), w_{,j}^{K}\right) + B_{K}\left(w^{K}\right),$$

$$\left(\left(\left(\frac{\mu_{0}}{\rho} + \frac{\mu_{t}}{\rho \sigma_{\varepsilon}}\right)\varepsilon_{,j}\right)_{,j}, w^{\varepsilon}\right) = -\left(\left(\left(\frac{\mu_{0}}{\rho} + \frac{\mu_{t}}{\rho \sigma_{\varepsilon}}\right)\varepsilon_{,j}\right), w_{,j}^{\varepsilon}\right) + B_{\varepsilon}\left(w^{\varepsilon}\right),$$

$$\left(\left(\left(\frac{\mu_{0}}{\rho} + \frac{\mu_{t}}{\rho \sigma_{\varepsilon}}\right)\varepsilon_{,j}\right)_{,j}, w^{\varepsilon}\right) = -\left(\left(\left(\frac{\mu_{0}}{\rho} + \frac{\mu_{t}}{\rho \sigma_{\varepsilon}}\right)\varepsilon_{,j}\right), w_{,j}^{\varepsilon}\right) + B_{\varepsilon}\left(w^{\varepsilon}\right),$$

$$\left(\left(\frac{\mu_{0}}{\rho} + \frac{\mu_{t}}{\rho \sigma_{\varepsilon}}\right)\varepsilon_{,j}\right)_{,j}, w^{\varepsilon}\right) = -\left(\left(\left(\frac{\mu_{0}}{\rho} + \frac{\mu_{t}}{\rho \sigma_{\varepsilon}}\right)\varepsilon_{,j}\right), w_{,j}^{\varepsilon}\right) + B_{\varepsilon}\left(w^{\varepsilon}\right),$$

$$\left(\left(\frac{\mu_{0}}{\rho} + \frac{\mu_{t}}{\rho \sigma_{\varepsilon}}\right)\varepsilon_{,j}\right)_{,j}, w^{\varepsilon}\right) = -\left(\left(\frac{\mu_{0}}{\rho} + \frac{\mu_{t}}{\rho \sigma_{\varepsilon}}\right)\varepsilon_{,j}\right), w_{,j}^{\varepsilon}\right) + B_{\varepsilon}\left(w^{\varepsilon}\right),$$

$$\left(\left(\frac{\mu_{0}}{\rho} + \frac{\mu_{t}}{\rho \sigma_{\varepsilon}}\right)\varepsilon_{,j}\right)_{,j}, w^{\varepsilon}\right) = -\left(\left(\frac{\mu_{0}}{\rho} + \frac{\mu_{t}}{\rho \sigma_{\varepsilon}}\right)\varepsilon_{,j}\right), w_{,j}^{\varepsilon}\right) + B_{\varepsilon}\left(w^{\varepsilon}\right),$$

$$\left(\left(\frac{\mu_{0}}{\rho} + \frac{\mu_{t}}{\rho \sigma_{\varepsilon}}\right)\varepsilon_{,j}\right)_{,j}, w^{\varepsilon}\right) = -\left(\left(\frac{\mu_{0}}{\rho} + \frac{\mu_{t}}{\rho \sigma_{\varepsilon}}\right)\varepsilon_{,j}\right), w_{,j}^{\varepsilon}\right) + B_{\varepsilon}\left(w^{\varepsilon}\right),$$

Fac. of Grad. Studies, Mahidol Univ.

where B_p, B_u, B_T, B_K , and B_{ε} are as follows

$$B_{p}(w^{u_{i}}) = \int_{\Gamma} \frac{1}{\rho} p^{*} w^{u_{i}} \cdot \mathbf{n} \, d\Gamma,$$

$$B_{u}(w^{u_{i}}) = \int_{\Gamma} \frac{\mu_{f}}{\rho} \left(u_{i,j} + u_{j,i} \right) w^{u_{i}} \cdot \mathbf{n} \, d\Gamma,$$

$$B_{T}(w^{T}) = \int_{\Gamma} \frac{k_{f}}{\rho c} T_{,j} w^{T} \cdot \mathbf{n} \, d\Gamma,$$

$$B_{K}(w^{K}) = \int_{\Gamma} \left(\frac{\mu_{0}}{\rho} + \frac{\mu_{t}}{\rho \sigma_{K}} \right) K_{,j} w^{K} \cdot \mathbf{n} \, d\Gamma,$$

$$B_{\varepsilon}(w^{\varepsilon}) = \int_{\Gamma} \left(\frac{\mu_{0}}{\rho} + \frac{\mu_{t}}{\rho \sigma_{\varepsilon}} \right) \varepsilon_{,j} w^{\varepsilon} \cdot \mathbf{n} \, d\Gamma.$$

$$(4.27)$$

To find the solution of the above VBVP problem, the Bubnov-Galerkin finite element method is used to solve the problem. The problem is posed into an N-dimensional subspace for u_i, T, K and ε and an N'-dimensional subspace for p^* . Let H_{γ} be an N-dimensional subspace of $H^1(\Omega)$ with basis functions $\{\gamma_1, \gamma_2, \dots, \gamma_n\}$ and H_{β} be an N'-dimensional subspace of $H^1(\Omega)$ with basis function $\{\beta_1, \beta_2, \dots, \beta_n\}$. Then $w^{u_i}, w^T, w^K, w^{\varepsilon}$ and w^p are approximated by

$$w^{u_i} \approx \hat{w}^{u_i} = \sum_{m=1}^{N} \gamma_m w_m^{u_i}, \quad w^T \approx \hat{w}^T = \sum_{m=1}^{N} \gamma_m w_m^T,$$

$$w^K \approx \hat{w}^K = \sum_{m=1}^{N} \gamma_m w_m^K, \quad w^\varepsilon \approx \hat{w}^\varepsilon = \sum_{m=1}^{N} \gamma_m w_m^\varepsilon,$$

$$w^p \approx \hat{w}^p = \sum_{p=1}^{N'} \beta_p w_p.$$

$$(4.28)$$

Substituting equations (4.26) - (4.28) into equation (4.24) and noting that the test function is arbitrary, we have

$$(u_{i,i},\beta_n) = -(\delta p^*,\beta_n),$$

$$\begin{split} \left(\frac{\partial u_{i}}{\partial t},\gamma_{m}\right) + \left(u_{j}u_{i,j},\gamma_{m}\right) + \left(\left(\frac{\mu_{f}}{\rho}\left(u_{i,j} + u_{j,i}\right)\right),\gamma_{m,j}\right) - \left(\frac{1}{\rho}p^{*},\gamma_{m,i}\right) \\ &= \left(\frac{1}{\rho}F_{i},\gamma_{m}\right) + \left(\frac{1}{\rho}F_{em_{i}},\gamma_{m}\right) + B_{u}(\gamma_{m}) - B_{p}(\gamma_{m}), \\ \left(\frac{\partial T}{\partial t},\gamma_{m}\right) + \left(u_{j}T_{,j},\gamma_{m}\right) + \left(\left(\frac{k_{f}}{\rho c}T_{,j}\right),\gamma_{m,j}\right) \\ &= -\frac{1}{c}\left\{\left(\frac{\partial H}{\partial t},\gamma_{m}\right) + \left(u_{j}H_{,j},\gamma_{m}\right)\right\} + B_{T}(\gamma_{m}), \\ \left(\frac{\partial K}{\partial t},\gamma_{m}\right) + \left(u_{j}K_{,j},\gamma_{m}\right) + \left(\left(\left(\frac{\mu_{0}}{\rho} + \frac{\mu_{t}}{\rho\sigma_{K}}\right)K_{,j}\right),\gamma_{m,j}\right) \\ &= -\left(\frac{\mu_{t}}{\rho\sigma_{t}}\beta g_{j}T_{,j} - \frac{\mu_{t}}{\rho}G + \varepsilon,\gamma_{m}\right) + B_{K}(\gamma_{m}), \\ \left(\frac{\partial \varepsilon}{\partial t},\gamma_{m}\right) + \left(u_{j}\varepsilon_{,j},\gamma_{m}\right) + \left(\left(\left(\frac{\mu_{0}}{\rho} + \frac{\mu_{t}}{\rho\sigma_{\varepsilon}}\right)\varepsilon_{,j}\right),\gamma_{m,j}\right) \\ &= \left(C_{1}(1 - C_{3})\frac{\varepsilon\mu_{t}}{K\rho\sigma_{t}}\beta g_{j}T_{,j} + C_{1}\frac{\varepsilon\mu_{t}}{K\rho}G - C_{2}f_{\varepsilon}\frac{\varepsilon^{2}}{K},\gamma_{m}\right) + B_{\varepsilon}(\gamma_{m}), \quad (4.29) \end{split}$$

Similarly, u_i, T, K, ε and p^* are approximated by

$$u_{i}(\mathbf{x},t) \approx \hat{u}_{i} = \sum_{l=1}^{N} (u_{i})_{l}(t)\gamma_{l}(\mathbf{x}),$$

$$T(\mathbf{x},t) \approx \hat{T} = \sum_{l=1}^{N} T_{l}(t)\gamma_{l}(\mathbf{x}),$$

$$K(\mathbf{x},t) \approx \hat{K} = \sum_{l=1}^{N} K_{l}(t)\gamma_{l}(\mathbf{x}),$$

$$\varepsilon(\mathbf{x},t) \approx \hat{\varepsilon} = \sum_{l=1}^{N} \varepsilon_{l}(t)\gamma_{l}(\mathbf{x}),$$

$$p^{*}(\mathbf{x},t) = \sum_{k=1}^{N'} p_{k}^{*}(t)\beta_{k}(\mathbf{x}).$$

$$(4.30)$$

Substituting equation (4.30) into equation (4.29), we have

$$\sum_{l=1}^{N} (\gamma_{l,i}, \beta_{p}) u_{il} = -\sum_{l=1}^{N'} (\delta \beta_{l}, \beta_{p}) p_{l}^{*},$$

$$\sum_{l=1}^{N} \left\{ (\gamma_{l}, \gamma_{m}) \dot{u}_{il} + (u_{j} \gamma_{l,j}, \gamma_{m}) u_{il} + \frac{\mu_{f}}{\rho} (\gamma_{l,j}, \gamma_{m,j}) u_{il} + \frac{\mu_{f}}{\rho} (\gamma_{l,i}, \gamma_{m,j}) u_{jl} \right\}
- \frac{1}{\rho} \sum_{l=1}^{N'} \left\{ (\beta_{l}, \gamma_{m,i}) p_{l}^{*} - \rho B_{p} (\gamma_{m}) \right\} = \left(\frac{1}{\rho} F_{i}, \gamma_{m} \right) + \left(\frac{1}{\rho} F_{em_{i}}, \gamma_{m} \right) + B_{u} (\gamma_{m}),
\sum_{l=1}^{N} \left\{ (\gamma_{l}, \gamma_{m}) \dot{T}_{l} + (u_{j} \gamma_{l,j}, \gamma_{m}) T_{l} + \left(\frac{k_{f}}{\rho c} \gamma_{l,j}, \gamma_{m,j} \right) T_{l} \right\} - B_{T} (\gamma_{m})
= -\frac{1}{c} \sum_{l=1}^{N} \left\{ (\gamma_{l}, \gamma_{m}) \dot{H}_{l} + (u_{j} \gamma_{l,j}, \gamma_{m}) H_{l} \right\},
\sum_{l=1}^{N} \left\{ (\gamma_{l}, \gamma_{m}) \dot{K}_{l} + (u_{j} \gamma_{l,j}, \gamma_{m}) K_{l} + \left(\left(\frac{\mu_{0}}{\rho} + \frac{\mu_{t}}{\rho \sigma_{K}} \right) \gamma_{l,j}, \gamma_{m,j} \right) K_{l} \right\}
= -\left(\frac{\mu_{t}}{\rho \sigma_{t}} \beta g_{j} T_{,j} - \frac{\mu_{t}}{\rho} G + \varepsilon, \gamma_{m} \right) + B_{K} (\gamma_{m}),
\sum_{l=1}^{N} \left\{ (\gamma_{l}, \gamma_{m}) \dot{\varepsilon}_{l} + (u_{j} \gamma_{l,j}, \gamma_{m}) \varepsilon_{l} + \left(\left(\frac{\mu_{0}}{\rho} + \frac{\mu_{t}}{\rho \sigma_{\varepsilon}} \right) \gamma_{l,j}, \gamma_{m,j} \right) \varepsilon_{l} \right\}
= \left(C_{1} (1 - C_{3}) \frac{\varepsilon \mu_{t}}{K \rho \sigma_{c}} \beta g_{j} T_{,j} + C_{1} \frac{\varepsilon \mu_{t}}{K \rho} G - C_{2} f_{\varepsilon} \frac{\varepsilon^{2}}{K}, \gamma_{m} \right) + B_{\varepsilon} (\gamma_{m}),$$
(4.31)

for m = 1, 2, 3, ..., N and p = 1, 2, 3, ..., N'. The Newmann type and Robin type boundary conditions in (4.18)-(4.21) can now be introduced into system (4.31). Thus, we have

$$B_{p}(\gamma_{m}) = \int_{\Gamma_{exit}} \frac{1}{\rho} \gamma_{m} \beta_{l} d\Gamma p_{l}^{*},$$

$$B_{T}(\gamma_{m}) = -\int_{\Gamma_{wall}} \frac{1}{\rho c} h_{\infty} \gamma_{l} \gamma_{m} d\Gamma T_{l} + \int_{\Gamma_{wall}} \frac{1}{\rho c} h_{\infty} \gamma_{m} T_{\infty} d\Gamma.$$

$$(4.32)$$

The system of equations (4.31) can be expressed in matrix form as follows

$$\begin{bmatrix} C_{1}^{T} & C_{2}^{T} \end{bmatrix} \begin{bmatrix} U_{1} \\ U_{2} \end{bmatrix} = -\delta M_{p} p^{*},$$

$$S\dot{U}_{i} + BU_{i} + A_{u_{i}}^{1} U_{1} + A_{u_{i}}^{2} U_{2} - C_{i}^{*} p^{*} = F_{u_{i}} + F_{em_{i}},$$

$$S\dot{T} + BT + A_{T}T + A_{b}T = F_{T} + S'\dot{H} + B'H,$$

$$S\dot{K} + BK + A_{K}K = F_{K},$$

$$S\dot{E} + BE + A_{\varepsilon}E = F_{\varepsilon},$$

$$(4.33)$$

From equation $(4.33)_1$, we can write p^* in terms of U_i as follow

$$p^* = -\frac{1}{\delta} M_p^{-1} \left(C_1^T U_1 + C_2^T U_2 \right).$$

Thus, the pressure term in the system of equations (4.33) can be eliminated so that we have

$$S\dot{U}_i + BU_i + A_{u_i}^1 U_1 + A_{u_i}^2 U_2 + \frac{1}{\delta} C_i^* M_p^{-1} \left(C_1^T U_1 + C_2^T U_2 \right) = F_{u_i} + F_{em_i}.$$
(4.34)

The system of equations (4.34) then can be written into two groups in matrix form

$$\begin{bmatrix} S & 0 & 0 \\ 0 & S & 0 \\ 0 & 0 & S \end{bmatrix} \begin{bmatrix} \dot{U}_1 \\ \dot{U}_2 \\ \dot{T} \end{bmatrix}$$

$$+ \begin{bmatrix} B + A_{u_1}^1 + \frac{1}{\delta} C_1^* M_p^{-1} C_1^T & A_{u_1}^1 + \frac{1}{\delta} C_1^* M_p^{-1} C_2^T & 0 \\ A_{u_2}^1 + \frac{1}{\delta} C_2^* M_p^{-1} C_1^T & B + A_{u_2}^1 + \frac{1}{\delta} C_2^* M_p^{-1} C_2^T & 0 \\ 0 & 0 & B + A_T + A_b \end{bmatrix} \begin{bmatrix} U_1 \\ U_2 \\ T \end{bmatrix}$$

$$= \begin{bmatrix} F_{u_1} \\ F_{u_2} \end{bmatrix} + \begin{bmatrix} F_{em_1} \\ F_{em_2} \end{bmatrix} + \begin{bmatrix} 0 \\ 0 \\ \vdots \end{bmatrix}, \quad (4.35)$$

Fac. of Grad. Studies, Mahidol Univ.

$$\begin{bmatrix} S & 0 \\ 0 & S \end{bmatrix} \begin{bmatrix} \dot{K} \\ \dot{E} \end{bmatrix} + \begin{bmatrix} B + A_k & 0 \\ 0 & B + A_{\varepsilon} \end{bmatrix} \begin{bmatrix} K \\ E \end{bmatrix} = \begin{bmatrix} F_K \\ F_{\varepsilon} \end{bmatrix}, \tag{4.36}$$

where the coefficient matrices are defined by

$$M_p = ((m_p)_{lm})_{N' \times N'} \quad \text{with} \quad (m_p)_{lm} = \int_{\Omega} \beta_l \beta_m \, d\Omega,$$

$$C_i = \left\{ c_{lm}^i \right\}_{N \times N'} \quad \text{with} \quad c_{lm}^i = \int_{\Omega} \frac{\partial \gamma_l}{\partial x_i} \beta_m \, d\Omega \quad (i = 1, 2),$$

$$C_i^* = \frac{1}{\rho} \left\{ c_{lm}^i - c_{lm}^* \right\}_{N \times N'} \quad \text{with} \quad c_{lm}^* = \int_{\Gamma_{exit}} \gamma_l \beta_m \, d\Gamma,$$

$$S = (s_{lm})_{N \times N}, S' = -\frac{1}{c}(s_{lm})_{N \times N}$$
 with $s_{lm} = \int_{\Omega} \gamma_l \gamma_m d\Omega$,

$$B = (b_{lm})_{N \times N}, B' = -\frac{1}{c}(b_{lm})_{N \times N} \quad \text{with} \quad b_{lm} = \int_{\Omega} \gamma_l(u_j \frac{\partial \gamma_m}{\partial x_j}) d\Omega, \quad (j = 1, 2)$$

$$A_{u} = \begin{bmatrix} A_{u_{1}}^{1} & A_{u_{1}}^{2} \\ A_{u_{2}}^{1} & A_{u_{2}}^{2} \end{bmatrix} = \begin{bmatrix} 2a_{lm}^{11} + d_{lm}^{22} & a_{lm}^{12} \\ a_{lm}^{21} & a_{lm}^{11} + 2a_{lm}^{22} \end{bmatrix}_{2N \times 2N} \text{ with } a_{lm}^{ij} = \int_{\Omega} \frac{\mu_{f}}{\rho} \frac{\partial \gamma_{l}}{\partial x_{i}} \frac{\partial \gamma_{m}}{\partial x_{j}} d\Omega ,$$

$$(i, j = 1, 2)$$

$$A_T = (a_{lm}^T)_{N \times N}$$
 with $a_{lm}^T = \int_{\Omega} \frac{k_f}{\rho c} (\frac{\partial \gamma_l}{\partial x_j} \frac{\partial \gamma_m}{\partial x_j}) d\Omega$; $(j = 1, 2)$,

$$A_k = (a_{lm}^k)_{N \times N}$$
 with $a_{lm}^k = \int_{\Omega} (\frac{\mu_0}{\rho} + \frac{\mu_t}{\rho \sigma_K}) (\frac{\partial \gamma_l}{\partial x_j} \frac{\partial \gamma_m}{\partial x_j}) d\Omega$; $(j = 1, 2)$,

$$A_{\varepsilon} = (a_{lm}^{\varepsilon})_{N \times N} \quad \text{with} \quad a_{lm}^{\varepsilon} = \int_{\Omega} (\frac{\mu_0}{\rho} + \frac{\mu_t}{\sigma_{\varepsilon}}) (\frac{\partial \gamma_l}{\partial x_j} \frac{\partial \gamma_m}{\partial x_j}) d\Omega \ ; (j = 1, 2),$$

$$F_{u} = \begin{bmatrix} f_{l}^{1} \\ f_{l}^{2} \end{bmatrix}_{2N \times 1} \quad \text{with} \quad f_{l}^{1} = \int_{\Omega} \frac{\mu_{f}}{\rho \kappa} u \gamma_{l} d\Omega, \quad f_{l}^{2} = \int_{\Omega} \frac{\mu_{f}}{\rho \kappa} (v - U_{cast}) \gamma_{l} d\Omega,$$

$$F_{em} = \begin{bmatrix} f_{em_l}^1 \\ f_{em_l}^2 \end{bmatrix}_{2N \times 1} \quad \text{with} \quad f_{em_l}^1 = \int_{\Omega} \frac{1}{\rho} F_{em_x} \gamma_l \, d\Omega, \quad f_{em_l}^2 = \int_{\Omega} \frac{1}{\rho} F_{em_z} \gamma_l \, d\Omega,$$

$$A_b = (a_{lm}^b)_{N \times N}$$
 with $a_{ij}^b = \frac{1}{\rho c} \int_{\Gamma_{wall}} h_{\infty} \gamma_l \gamma_m \, d\Gamma$,

$$F_T = (f_l^T)_{N \times 1} \text{ with } f_l^T = \frac{1}{\rho c} \int_{\Gamma_{woll}} h_{\infty} T_{\infty} \gamma_l d\Gamma,$$

$$F_K = (f_l^K)_{N \times 1}$$
 with $f_l^K = \int_{\Omega} (\nu_t G - \varepsilon - \frac{\nu_t}{\sigma_t} \beta g \frac{\partial T}{\partial z}) \gamma_l \, d\Omega$,

$$F_{\varepsilon} = (f_l^{\varepsilon})_{N \times 1} \quad \text{with} \quad f_l^{\varepsilon} = \int_{\Omega} (C_1 \frac{\varepsilon}{K} \nu_t G + C_1 (1 - C_3) \frac{\varepsilon \nu_t}{K \sigma_t} \beta g \frac{\partial T}{\partial z} - C_2 f_{\varepsilon} \frac{\varepsilon^2}{K}) \gamma_l \, d\Omega.$$

$$(4.37)$$

To find the finite element solutions of (4.35) and (4.36), we discretize the computation domain Ω into M elements Ω_e , namely

$$\Omega = \bigcup_{e=1}^{M} \Omega_e,$$

where $\Omega_i \cap \Omega_j = 0 \ \forall i \neq j$. The basis functions $\gamma_l(\mathbf{x}_j)$ are chosen to be piecewise continuous and to have a value of one at its their node and zero at other nodes. Then, the integral terms defined in (4.37) can be obtained by assembling the contribution from each element. For example,

$$\int_{\Omega} \gamma_l \gamma_m \, d\Omega = \sum_{e=1}^{M} \int_{\Omega_e} \gamma_l^e \gamma_m^e \, d\Omega_e. \tag{4.38}$$